PHYSICAL REVIEW C VOLUME 23, NUMBER 2 FEBRUARY 1981

Projectile breakup reaction and evidence of a breakup-fusion mechanism

E. Takada,* T. Shimoda,† N. Takahashi,‡ T. Yamaya,§ and K. Nagatani
Cyclotron Institute, Texas A&M University, College Station, Texas 77843

T. Udagawa and T. Tamura
Department of Physics, University of Texas, Austin, Texas 78712
(Received 10 September 1980)

Coincidence measurement was made in the reaction $^{40}Ca(^{20}Ne,^{16}O\alpha)$ at 260 MeV incident energy, and the experimental results were analyzed in terms of the projectile breakup scheme. The reaction can be conveniently classified into the elastic- and inelastic-breakup processes. Comparison of the present results to those of the ^{16}O-singles measurement indicates the importance of the process in which the breakup is followed by the fusion process. Theoretical analysis shows that the main aspects of the present experimental results are explained.

[NUCLEAR REACTIONS $^{40}Ca(^{20}Ne,^{16}O\alpha)$ $E=260$ MeV measured coincidence energy and angular correlations. Deduce reaction mechanisms. Calculations of elastic breakup and breakup-fusion processes.]

I. INTRODUCTION

In a recent study, we reported[1] the results of the singles measurements of three different reactions, (^{13}C, ^{9}Be), (^{14}N, ^{10}B), and (^{20}Ne, ^{16}O), on the ^{40}Ca target at about 10 MeV/nucleon incident energies. The experimental results were analyzed by assuming the α-transfer mechanism with the use of the distorted-wave Born approximation. For the first two reactions, the theoretical analyses successfully reproduced the entire shapes of the continuum energy spectra, which span wide energy ranges up to more than 100 MeV excitation in the residual nuclear systems, and also explained the angular distributions.

It was noticed, however, that the spectra of the last reaction, (^{20}Ne, ^{16}O), show a characteristically different feature from the other two reactions. In addition to the same broadly distributed component, there clearly appears an extra component which has a narrower width and a peak position at about $\frac{16}{20}$ of the incident energy, irrespective to observed angles. The angular distribution of this extra component is also very different; it is very strong in forward angles and decreases quite rapidly with increasing angles. For instance, at 5° the strength of this component is almost five times larger than the rest, and at 15° it disappears leaving the spectra similar to those of the other reactions.

Based on these findings, we conjectured that this extra component comes from a projectile breakup process. This conjecture was first tested[2] experimentally by investigating these three reactions on different target nuclei, i.e., ^{58}Ni and ^{94}Mo, since the projectile breakup reaction should be insensitive to a choice of target nuclei. As expected, we found that the same feature persisted in these reactions; the (^{20}Ne, ^{16}O) reaction uniquely displayed this extra component. Actual theoretical analyses were subsequently performed[3] by assuming a breakup of ^{20}Ne into ^{16}O and an α particle through an inelastic excitation of ^{20}Ne. The numerical calculations reproduced simultaneously the shape of this extra component of the spectra and its angular distribution. Therefore, the observed results of the ^{16}O-singles measurement were explained by superimposing the breakup process on the transfer process.

In the present investigation, we extended the study by performing coincidence measurements of ^{16}O and the α particle induced by the bombardment of ^{40}Ca with 260 MeV ^{20}Ne. The result of the present observation revealed several important features not noticed in the singles measurement, which provided more subtle information for the reaction mechanism. As a consequence, the theoretical treatment has been extended to explain these additional features.

The experimental result first showed that the coincidence events are concentrated in the kinematical region where the three final particles are in their ground states. The spectra projected to the ^{16}O-energy axis from this region show the same shape as the component attributed to the breakup process in the singles spectra. It was further noticed that a fairly large number of events fall in a wide energy region of excited final states and display a similar shape to the transfer component of the singles spectra. From these observations, we define these two components in the coincidence spectra to be the "elastic-breakup" and "inelastic-breakup" processes. It is obvious that the elastic breakup corresponds to a

part of the breakup component in the singles spectra, while the inelastic breakup component constitutes a part of the transfer spectrum.

Finally, the present result demonstrated another important feature. The coincidence cross section of the elastic-breakup component was found to be smaller than that of the breakup part of the ^{16}O-singles spectra by a considerable factor. In other words, a major part of the ^{16}O-singles strength does not accompany the α particle. A similar but even more drastic reduction in the coincidence cross section was observed when the α-particle spectra were compared. A straightforward interpretation of these missing strengths in the coincidence cross sections is that they are caused by an absorption of a breakup particle by the target nucleus. For instance, when ^{16}O is detected, the absorption of α particles into ^{40}Ca reduces the coincidence yield but not the singles yield. The larger reduction observed in the α-particle detection can then be attributed to a stronger absorptive interaction of ^{16}O with ^{40}Ca A theoretical formulation and actual analysis for the elastic-breakup process has been carried out by considering the absorption in terms of the fusion mechanism. We define this mechanism to be the "breakup fusion" process. (Bauer *et al.*[4] call it the inelastic breakup process.)

In Sec. II, we describe briefly the experimental procedures. The experimental results are presented in Sec. III, together with discussions to clarify the observed results in terms of the breakup model. The discussion then leads to a necessary extension of the model to include the breakup fusion process which is described in Sec. IV. In Sec. V, the concluding remarks are given.

II. EXPERIMENTAL PROCEDURES

A beam of 262 MeV ^{20}Ne^{6+} was extracted from the Texas A & M cyclotron. Since spectra were all continuum spectra, special care was taken in the collimation of the beam by using a set of defining and antiscattering slits to avoid problems associated with stray beams. The beam intensity was typically 100 nA (current) on the target, which was collected in a Faraday cup, and a monitor counter was also used. The target was a self-supporting natural calcium of 2.3 mg/cm^2 thickness, and the incident energy was estimated to be 260 MeV at the center of the target. To minimize contaminants, the target was freshly made just before the runs and transported in an argon environment. Contaminants were monitored during the runs by observing the elastic and inelastic spectra and were determined to be negligible.

Two solid-state counter telescopes were used to detect heavy ions and α particles separately. The detectors used for the heavy ion were 92.6 μm ΔE and 1022 μm E; for the α-particle detections, they were 53.1 and 3000 μm, respectively. The defining slit for the heavy-ion counter was 8.0 mm in diameter, providing the solid angle of 1.8 msr, while those for the α counter were 5.0 mm and 1.5 msr. The effect of these finite angular openings was taken into account in the final analysis of the cross sections in the coincidence data. Conventional electronics and an on-line PDP-15 computer provided the data acquisition system, and the particle identifications were made using a software program.[5]

The experiment was not designed to obtain particularly high energy resolution, since the spectra of interest were all continuum. In fact, the resolution of the elastic peak was typically 1.2 MeV determined mainly by the large angular opening. It would be larger for α-particle spectra because of the large difference in the energy losses of heavy ions and α particles in the target. The accuracy of the absolute cross sections was estimated to be within $\pm$ 20% due to uncertainties in the beam collection, target thickness, estimates of the solid angles, etc., the relative cross sections were believed to be accurate within the statistical errors. The measurements were carried out for the ^{16}O angle of 7.0° and 9.0°, and the α counter was set at −9.0°, −13.5°, −17.5°, −21.5°, and + 20.0°, where the negative angles specify the opposite side of the beam axis from the ^{16}O counter.

III. EXPERIMENTAL RESULTS AND DISCUSSIONS

In this section, the experimental results are presented. Discussions are also given to clarify the observed features of the elastic-breakup component in terms of the previously developed breakup theory.[3] As to the inelastic-breakup component, the theoretical analysis has not been made, thus we will not elaborate but just present the experimental results.

In Fig. 1, an example of the measured two-dimensional coincidence ^{16}O-α energy spectra taken at $\theta_{^{16}O} = 9°$ and $\theta_\alpha = -9°$ is shown. The straight line drawn in Fig. 1 indicates a kinematic locus for the reaction in which three final particles are all in their ground states. Here we introduce a breakup Q value Q_3' as $Q_3' = Q_3 + 4.73$ MeV, where Q_3 is the three-body reaction Q value and 4.73 MeV is the separation energy of ^{20}Ne into ^{16}O and an α particle; thus the line represents $Q_3' = 0$. The events along this locus correspond to the elastic-breakup component. A strong concentration of the yield along this line clearly indicates a large cross

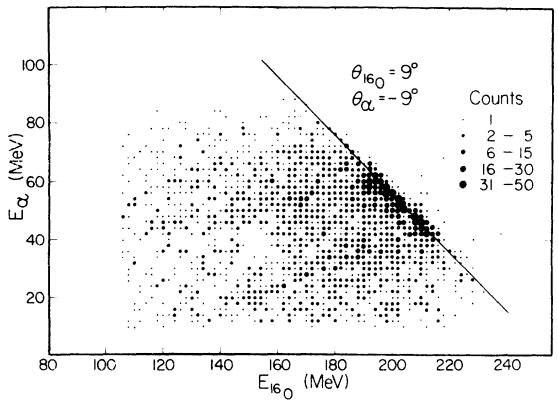

FIG. 1. Two-dimensional spectrum taken at $\theta_{^{16}O} = 9.0°$ and $\theta_\alpha = -9.0°$. Count in each channel is indicated by the size of the dot, and the solid line shows the kinematical locus for $Q_3' = 0$.

section of the elastic-breakup process at this angular configuration. It is also seen that there is an equally strong yield which corresponds to the inelastic-breakup process, but these events lie in a much wider range of $E_{^{16}O}$ and E_α with less concentration.

In order to relate the present data to the result of the singles measurement,[1] we first construct the ^{16}O-energy spectra by projecting the two-dimensional spectra onto the $E_{^{16}O}$ axis. In Fig. 2, such spectra are shown, and for comparison, the ^{16}O-singles spectra are displayed in the top. The spectrum shape is quite similar to that of the singles spectra: The breakup peak appears at the high energy end, while a broader transferlike spectrum is seen in the low energy region. It is important to remark that these breakup and transferlike spectra essentially come from elastic and inelastic components of the coincidence events, respectively.

To further inspect the reaction mechanism, it is instructive to examine the data in terms of various kinematical behavior. Since the coincidence detection of ^{16}O and the α particle completely determine the kinematical condition of this three-body reaction, we can introduce other kinematical variables into the spectrum. In Fig. 3, the two-dimensional spectrum is resketched schematically, and three kinematical variables are displayed. The solid lines indicate the kinematical loci for $Q_3' = 0$, -25, and -50 MeV. Events can also be labeled in terms of the excitation energy in the ^{20}Ne system, E_x(Ne), as indicated by the dashed curves. Furthermore, the scattering angle of the outgoing ^{20}Ne, θ_{Ne}, which is the center of mass of the outgoing ^{16}O and α particle, can de determined as shown by the dotted

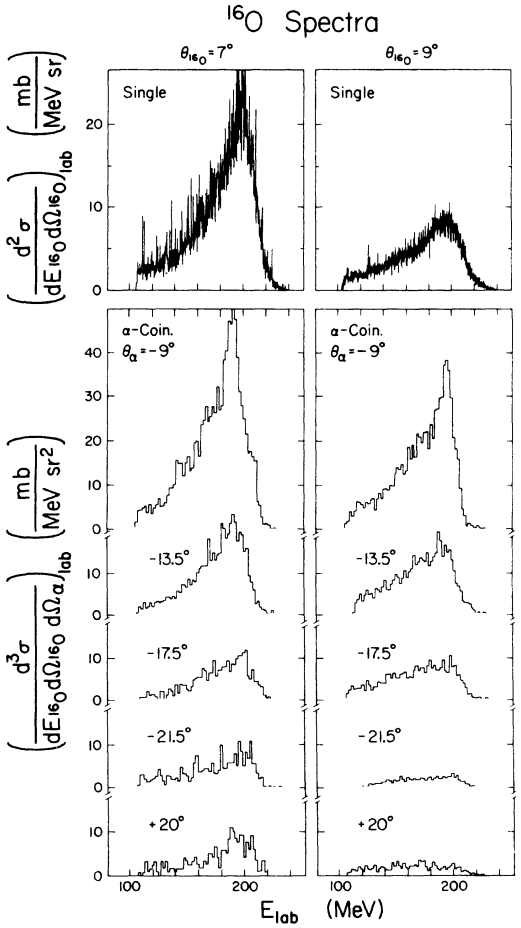

FIG. 2. Singles and coincidence spectra taken at $\theta_{^{16}O} = 7.0°$ and $9.0°$. The singles spectra are shown in the top, and the coincidence spectra projected onto the $E_{^{16}O}$ axis are displayed with θ_α labeled.

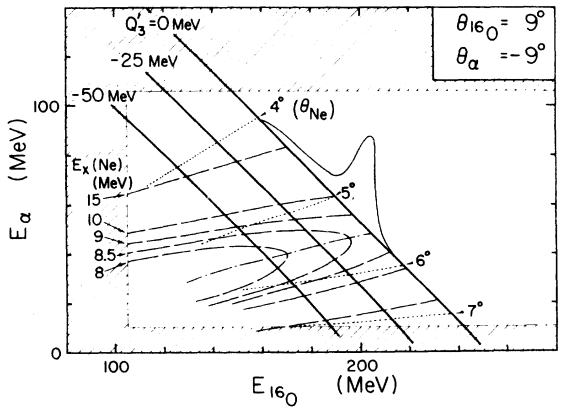

FIG. 3. Schematic diagram for various kinematical variables. The two-dimensional spectrum is schematically sketched, the elastic-breakup spectrum is illustrated in a three-dimensional peak, while the kinematical loci for Q_3' (solid curves), E_x(Ne) (dashed curves), and θ_{Ne} (dotted curves) are drawn in the $E_{^{16}O} - E_\alpha$ plane.

curves. The spectrum can then be reanalyzed in terms of these variables, and Fig. 4 shows such spectra. Figure 4(a) simply illustrates the $Q_3'=0$ locus in the E_x(Ne) and θ_{Ne} plane. Figures 4(b) and 4(c) show the actual spectra projected onto E_x(Ne) and θ_{Ne}, respectively.

An important characteristic of the elastic breakup mechanism can be learned from the spectrum shown in Fig. 4(b). It is clearly seen that the transition strength is strongly localized in the low E_x(Ne) region. The physical meaning of this feature can be readily understood. The inelastic transition strength of the ^{20}Ne is strongly governed by the ordinary Q value and transferred angular momentum effect as in any heavy-ion reactions. This effect, which is essentially a consequence of the momentum matching conditions, favors transitions to low excitation for low-spin transfer. The breakup strength is also affected by another factor reflecting the Coulomb and centrifugal barrier. When the projectile is excited to a scattering state, it has to proceed to the asymptotic region of ^{16}O and the α particle, for which the Coulomb barrier suppresses the low energy part. The theoretical calculation[3] in fact had exactly predicted this characteristic. The

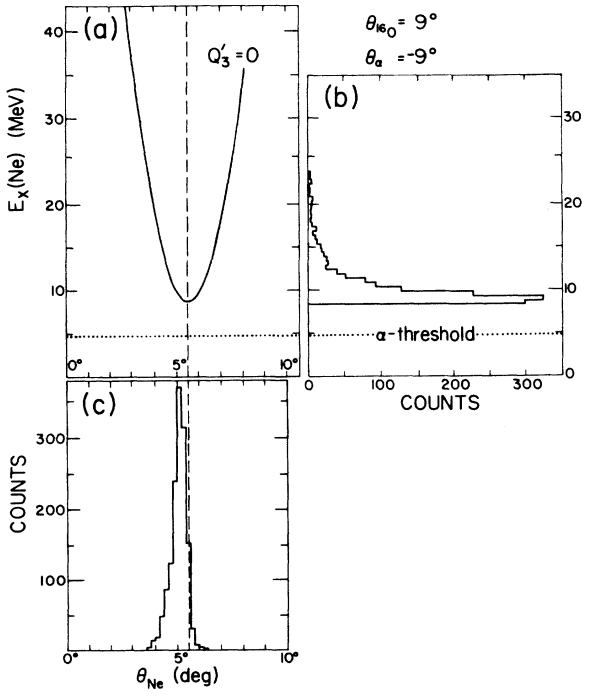

FIG. 4. θ_{Ne}–E_x(Ne) diagram for the $Q_3'=0$, elastic-breakup component: In (a) the Q_3' locus is shown in the θ_{Ne}–E_x(Ne) plane; in (b), the actual spectrum of the elastic-breakup process is shown in terms of E_x(Ne); and in (c), it is displayed as the function of θ_{Ne}.

calculated result showed that the process proceeds through a narrow region of the ^{20}Ne excitation peaking at about 8.7 MeV of E_x(Ne) (see Fig. 1 in Ref. 3). Therefore, the spectrum shown in Fig. 4(b) can be understood, though the behavior of the lower E_x(Ne) region is not tested from this experiment by the kinematical restriction. Detections of the lower E_x(Ne) region could have been possible only if the counters were set at much more forward angles, but it was practically impossible.

The spectrum projected onto the θ_{Ne} axis shown in Fig. 4(c) is considered next. From Fig. 4(a), it is seen that the $Q_3'=0$ locus provides a double value in θ_{Ne} for a given E_x(Ne). For this angular configuration, $\theta_{^{16}O}=9.0°$ and $\theta_\alpha=-9.0°$, θ_{Ne} is centered at 5.6° as indicated by the dashed line in Fig. 4(a) down to 4(c). Since the inelastic scattering of ^{20}Ne has a sharply rising angular distribution toward the forward angle, the spectrum shape tends to shift to the smaller θ_{Ne} side. In addition, the finite angular opening effectively integrates the yield in θ_{Ne} again favoring the smaller angle. The actual spectrum shown in Fig. 4(c) manipulates such a feature by having the peak shifted to the smaller θ_{Ne}. From these discussions, it is demonstrated that the observed feature of the elastic breakup component can be understood in the scheme of the breakup theory.

Finally, we analyze the spectra in terms of Q_3' as shown in Fig. 5, which is the most convenient format to consider the result in terms of the elastic- and inelastic-breakup processes. The prominence of the elastic-breakup peak is again clear. However, these spectra show complications in the vicinity of the elastic-breakup peak. There is a weak but definite indication of an enhancement at $Q_3'\approx -6$ MeV, which suggests transitions involving ^{16}O in the excited states at about 6 MeV. Furthermore, there may be a component appearing as a shoulder in the lower side of the elastic-breakup peak, which must then correspond to events with low-lying excited states of ^{40}Ca in the region of 3–4 MeV. Experimental separations of these transitions were not practically possible. It is even worse in the singles measurement where the separations are inherently impossible. Since the original definition of the elastic breakup, to which the theory is applied, is restricted to the process with $Q_3'=0$ transition, certain ambiguities are inevitably introduced in comparisons between the experimental and theoretical results.

From these spectra shown in Fig. 5, the cross sections for the elastic-breakup component can be extracted by integrating the spectra with respect to Q_3' in the region of the elastic-breakup peak. The summary of such cross sections is listed in

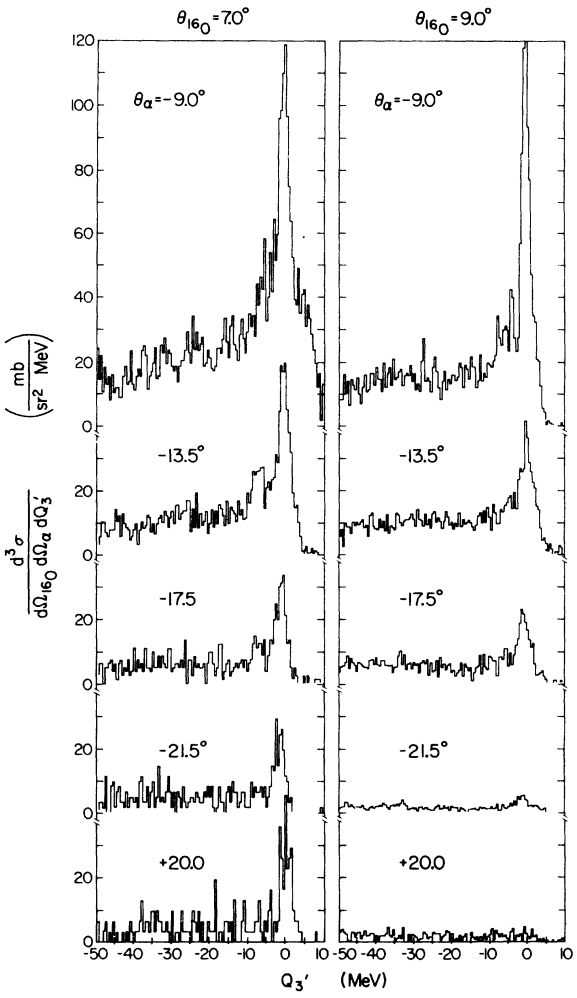

FIG. 5. Coincidence spectra projected onto the Q_3' axis; the same spectra shown in Fig. 2 are displayed in terms of Q_3'. Note the structure indicating an enhancement at about $Q_3' = -6$ MeV and the shoulder at about $Q_3' = -3$ MeV.

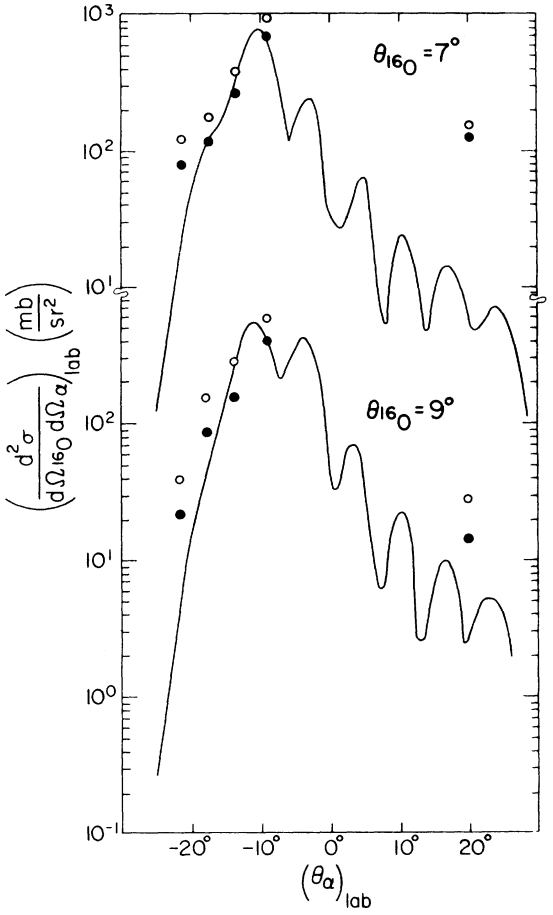

FIG. 6. Angular correlations. The solid points show the cross section of the elastic-breakup component, which were obtained by integrating the spectra shown in Fig. 5 for the region $Q_3' > -2.5$ MeV, while the open circles show those for the region $Q_3' > -10.0$ MeV. The solid curves are the theoretical results normalized to the solid points as seen.

TABLE I. Coincidence cross section of ^{40}Ca(^{20}Ne, ^{16}Oα) at $E_{lab} = 260$ MeV. Q_3' is the Q value measured from the breakup threshold. The unit is in mb/sr^2.

θ_{16O}	θ_α	$Q_3' > -2.5$ MeV	$Q_3' > -10.0$ MeV	$Q_3' < -10.0$ MeV	Total
7.0°	−9.0°	698.8	984.8	1073.2	2058.0
	−13.5°	243.0	406.9	619.1	1026.0
	−17.5°	110.3	185.4	362.1	547.5
	−21.5°	77.8	123.7	343.9	467.6
	+20.0°	124.3	165.2	250.2	415.4
9.0°	−9.0°	395.7	602.6	915.4	1518.0
	−13.5°	171.3	278.1	610.7	888.8
	−17.5°	96.4	151.5	408.4	559.9
	−21.5°	23.3	37.0	114.7	151.7
	+20.0°	13.4	28.9	143.1	172.0

Table I. Considering the ambiguities mentioned above, we extracted the cross sections for the elastic-breakup component in two different regions of the integrations for each angle, i.e., for the regions of $Q_3' > -2.5$ MeV and $Q_3' > -10.0$ MeV. The first choice of −2.5 MeV was made to exclude these low-lying excited states as much as possible. It should be noted, however, that such a tight restriction must underestimate these cross sections, considering the actual energy resolution. The second choice of −10.0 MeV, on the other hand, certainly includes these mixtures resulting in overestimates. The inelastic breakup and the total cross sections are listed in the fifth and the last columns, respectively.

In Fig. 6, these cross sections of the elastic-breakup component are plotted to show the angular correlations. The solid points correspond to the experimental cross sections integrated in the region of $Q_3' > -2.5$ MeV, and the open circles are those in the region of $Q_3' > -10.0$ MeV. The solid curves are the results of the theoretical calculation normalized to the experimental value at the maximum cross sections (solid points) as seen. The overall agreement of the theoretical results is good except in the large α-particle angles. The theoretical calculation shows very small out-of-plane yields, for which no experimental measurements were made.

We have presented the experimental results of the coincidence measurement. Most of the observed features of the elastic-breakup component have been successfully interpreted in the scheme of the breakup theory. However, we have discovered a serious problem in explaining the ratios of the observed coincidence and singles cross sections as already mentioned in the Introduction. In the next section, we describe the breakup-fusion process which was invoked to explain such ratios.

IV. BREAKUP-FUSION PROCESS

In this section, we first outline the breakup fusion process. Comparisons to the experimental results are then presented. The discussion is restricted to the elastic-breakup process, since actual analyses of the inelastic-breakup process have not been carried out yet; however, its extension to the inelastic-breakup process is in principle straightforward.

The process may be schematically described as

$$^{40}\mathrm{Ca}+{}^{20}\mathrm{Ne}-\begin{cases}{}^{40}\mathrm{Ca}+\alpha+{}^{16}\mathrm{O}, & \text{elastic breakup}\\ {}^{40}\mathrm{Ca}+\alpha+{}^{16}\mathrm{O}-{}^{44}\mathrm{Ti}^*+{}^{16}\mathrm{O}-\mathrm{C}+y+{}^{16}\mathrm{O}, & \text{elastic breakup fusion}.\end{cases} \tag{1}$$

In the second line, C and y are the final products emerging from the compound nucleus ^{44}Ti*.

Recently, Kerman and McVoy[6] presented a rather general formalism for the breakup-fusion process. Based on their treatment, a slight but significant modification has been made[7,8] to apply the theory for heavy-ion reactions. Since the detail has already been described,[7] and it is quite involved, only a brief illustration is given here.

The singles cross section for both the breakup and breakup-fusion processes can be given by

$$\frac{d^2\sigma}{dE_b d\Omega_b}=\frac{m_a m_b}{(2\pi\hbar)^2}\left(\frac{k_b}{k_a}\right)\sum_l A_l \sum_m |\beta_{lm}(\vec{k}_b)|^2 \tag{2}$$

if the factor A_l is understood as

$$A_l=\begin{cases}1, & \text{breakup} \quad (3a)\\ P_l/|S_l|^2, & \text{breakup fusion} \quad (3b)\end{cases}$$

(see Ref. 9). In Eq. (2), a and b denote the projectile (^{20}Ne) and the detected (^{16}O) particles, respectively, and $\beta_{lm}(\vec{k}_b)$ is the amplitude of the breakup process with the breakup α particle having the angular momentum (l,m) relative to the target nucleus, $\vec{k}_b$ being the momentum of the particle b. The factor P_l represents the penetrability of the α particle to the target nucleus, while S_l is the S-matrix element for the elastic scattering of the α particle on the target nucleus.

The appearance of the factor $|S_l|^{-2}$ in Eq. (3b) may be physically understood. The amplitude β_{lm} represents the breakup flux including the absorption in the final channel optical potential. However, a part of this absorption, i.e., the absorption of the α particle by the target nucleus, must be removed because the fusion term takes it into account. Therefore, the amplitude before this absorption is first calculated, which in turn corresponds to $\beta_{lm}/|S_l|$. The penetrability P_l then takes care of the absorption for the broken-up α particle into the fusion.

The amplitude β_{lm} can be calculated from the breakup amplitude T obtained in Ref. 3 by assuming the inelastic excitation of the projectile ^{20}Ne into its continuum state ^{20}Ne* (= ^{16}O + α), i.e.,

$$\beta_{lm}(\vec{k}_b)=\int T(\vec{k}_{a'},\vec{k}_{x'})Y_{lm}^*(\hat{k}_\alpha)d\hat{k}_\alpha, \tag{4}$$

where $T(\vec{k}_{a'},\vec{k}_{x'})$ is first obtained as a function of $\vec{k}_{a'}$ and $\vec{k}_{x'}$. The subscripts a' and x' denote the momenta between ^{20}Ne* and the target, and the α particle and ^{16}O, respectively. The momentum between the α particle and the target is represented by $\vec{k}_\alpha$. Using the simple relationship between

these momenta ($\vec{k}_{a'}, \vec{k}_{r'}$) and ($\vec{k}_b, \vec{k}_\alpha$), the calculation of Eq. (4) can be carried out.

We have used the well known parametrized forms for P_l and S_l, i.e.,

$$S_l = S_0 + (1 - S_0)\{1 + \exp[-(l - l_s)/\Delta]\}^{-1} \quad (5)$$

and

$$P_l = 1 - \{1 + \exp[-(l - l_{cr})/\Delta]\}^{-2}. \quad (6)$$

The critical angular momentum l_{cr} and Δ in Eq. (6) were calculated using the resonable set of the optical parameters of the α particle on ^{40}Ca; the values thus obtained where $l_{cr} = 6.5 + 0.217 E_\alpha$, $\Delta = 1.0$. E_α is the relative kinetic energy between the breakup α particle and the target nucleus. In Eq. (5), S_0 denotes the S matrix for $l = 0$. In the course of the analyses,[8] we found it more appropriate to reproduce the experimental results to adopt l_β instead of l_s, where l_β corresponds to the angular momentum producing the maximum $|\beta_{lm}|$. The values were $S_0 = 0.080$, $\Delta = 3.0$, and $l_\beta = 10.0 + 0.24 E_\alpha$.

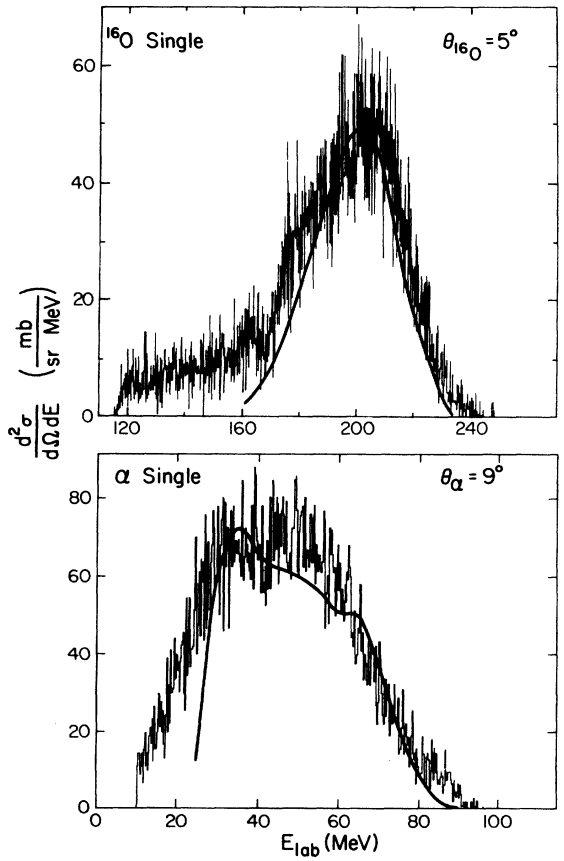

FIG. 7. Comparisons of the singles spectra to the theoretical results including the breakup fusion. The solid curves show the calculated spectra normalized to the experimental spectra.

The inclusion of this breakup-fusion term [Eq. 3(b)] modifies the theoretical predictions with the breakup term [Eq. 3(a)] alone. Numerical calculations have been carried out. It was found that the spectrum shape differs very little from the previously calculated spectra without the breakup-fusion term.[3] Thus an example of the ^{16}O-singles spectra is shown in Fig. 7 where the magnitude is normalized to the experimental spectrum. Using the same formalisms, the α-particle spectrum is also calculated and shown in Fig. 7. The theoretical spectrum shows the enhancements at about 35 and 65 MeV. The cause for these structures can be traced to the sharp cutoff of the breakup amplitude in the low E_x(Ne) region below the Coulomb barrier, as discussed in Ref. 3. The effect is strongly amplified in the α-particle spectrum compared to the ^{16}O spectrum. Before we make the final conclusion, however, there should be many more detailed examinations of various factors neglected here, such as the contributions and their interferences of higher l-wave excitations in ^{20}Ne, and those of the complete fusion process of the ^{20}Ne+^{40}Ca system. We believe that the shape in the high E_α region is, on the other hand, relatively free from these effects and well explained.

The significant effect of this additional breakup-fusion term appears in the magnitudes of cross sections. Although it is difficult to calculate the absolute cross sections very accurately, it is possible to obtain reliable values for the relative magnitude of the coincidence and singles spectra. Thus we are concerned here only with these relative magnitudes. When the angular correlations shown in Fig. 6 are integrated with respect to the α-particle angles, we obtain the cross section of the elastic breakup ^{16}O which is accompanied by the α particle, i.e., $(d\sigma/d\Omega_{^{16}O})_{coin}$. If the breakup-fusion process is absent, this cross section should be identical to that of the ^{16}O-singles spectrum integrated in the region of high energy peak with respect to the ^{16}O energy, i.e., $(d\sigma/d\Omega_{^{16}O})_{sing}$.

Such comparisons are shown in Table II. It should be noted that these values include large ambiguities. In particular, the values for $(d\sigma/d\Omega_{^{16}O})_{coin}$ are estimated by using the the-

TABLE II. Cross section of (^{20}Ne, ^{16}O) and ratios. The unit is in mb/sr for the cross sections.

$\theta_{^{16}O}$	$\left(\frac{d\sigma}{d\Omega_{^{16}O}}\right)_{sing}$	$\left(\frac{d\sigma}{d\Omega_{^{16}O}}\right)_{coin}$	Expt.[a]	Theor.
7.0°	420	70	6.0	5.8
9.0°	160	22	7.3	6.7

[a] The ratio $(d\sigma/d\Omega_{^{16}O})_{sing}/(d\sigma/d\Omega_{^{16}O})_{coin}$.

oretical angular correlation curve shown in Fig. 6, since it was not feasible to obtain the totally experimental cross sections by measuring the complete angular correlations. Furthermore, the extraction of the singles cross section $(d\sigma/d\Omega_{^{16}O})_{sing}$ also includes certain ambiguities due to complications, such as a separation from the transfer and inelastic-breakup components, inclusion of low-lying excited states as mentioned, etc. Nevertheless, it is obvious that there is a large difference in these coincidence and singles cross sections. In the fourth column in Table II, the ratios thus obtained are listed as "expt." The theoretical ratios including the breakup-fusion term are listed as "theo." The theoretical values are also to be subjected to various uncertainties involved. However, we believe that the general trend of this large difference in the coincidence and singles cross sections is nicely understood.

V. CONCLUSION

The coincidence measurement of ^{16}O and the α particle induced by the 260 MeV ^{20}Ne bombardment of ^{40}Ca was carried out. The spectra show the elastic- and inelastic-breakup events which demonstrate characteristically different features. In particular, the elastic-breakup events appear to be a strong peak in the high ^{16}O energy region, which in turn is identified to be the breakup component in the previous ^{16}O-singles spectra. The spectrum shape and the angular correlation pattern for the elastic breakup were well reproduced by the simple breakup calculation. However, the inclusion of the breakup-fusion process is necessary to explain the observed missing strength in the coincidence cross section when this cross section is compared to the singles ^{16}O cross section. This finding shows that the breakup process is quite dominant in the forward angles, but the absorption (or fusion) of the breakup particles with the target is also very important. The effect is more dramatically demonstrated in the α-particle spectra due to a stronger absorption of ^{16}O. The ratio of the theoretical results of the elastic-breakup and breakup-fusion cross sections for the singles spectra was found to be about 20.

In the present study, we have performed the theoretical analysis only for the elastic-breakup process. It will be most interesting to extend the study to the inelastic-breakup process. We also note that the present study has a direct relationship to the investigation of the so-called massive transfer reactions in which the formation of high-spin states is achieved and identified by detecting high energy α particles and γ rays in coincidence. In fact, the same theory has been recently applied to such experimental results, and successful interpretation was made.[8] An application of this model to the study of incident energy dependence of heavy-ion reactions is very interesting. We have already made a preliminary investigation for the reaction (^{16}O, ^{12}C) with the incident energies from about 10 to 20 MeV/nucleon.[10] It was clearly seen that the dominance of the elastic-breakup process becomes progressively larger as the incident energy is increased. Such studies should provide a wide scope of understanding of the heavy-ion reaction mechanism.

The present work was supported in part by the National Science Foundation and the U. S. Department of Energy.

---

*Permanent address: Department of Physics, Kyoto University, Kyoto, Japan.
†Present address: Department of Physics, Osaka University, Osaka, Japan.
‡Permanent address: Department of Physics, University of Tokyo, Tokyo, Japan.
§Present address: Department of Physics, Tohoku University, Sendai, Japan.

[1]H. Fröhlich, T. Shimoda, M. Ishihara, K. Nagatani, T. Udagawa, and T. Tamura, Phys. Rev. Lett. 42, 1518 (1979).
[2]T. Shimoda, Ph.D. thesis, Kyoto University, 1980 (unpublished).
[3]T. Udagawa, T. Tamura, T. Shimoda, H. Fröhlich, M. Ishihara, and K. Nagatani, Phys. Rev. C 20, 1949 (1979).
[4]G. Baur and D. Trautmann, Phys. Rep. 25C, 293 (1976); G. Baur, F. Rösel, D. Trautmann, and R. Shyam, in *Continuum Spectra on Heavy-Ion Reactions*, edited by T. Tamura, J. B. Natowitz, and D. H. Youngblood (Harwood, New York, 1980), p. 131.
[5]T. Shimoda, M. Ishihara, K. Nagatani, and T. Nomura, Nucl. Instrum. Methods 165, 261 (1979).
[6]A. K. Kerman and K. W. McVoy, Ann. Phys. (N.Y.) 122, 197 (1979).
[7]T. Udagawa and T. Tamura, Proceedings of the Research Center for Nuclear Physics—KIKUCHI Summer School on Nuclear Physics, Osaka, Japan, 1980 (unpublished).
[8]T. Udagawa and T. Tamura, Phys. Rev. Lett. 45, 1311 (1980).
[9]It is to be noted that a replacement $A_l = P_l/4$ in Eq. (3b) reduces the present formula to that derived by Kerman and McVoy. This difference is due to the inclusion of the off-the-energy shell and absorption effects here.
[10]E. Takada, N. Takahashi, T. Yamaya, T. Shimoda, K. Nagatani, T. Udagawa, and T. Tamura, Proceedings of the International Conference on Nuclear Physics, Berkeley, 1980 (LBL-11118), p. 621.